Available online at www.sciencedirect.com
SCIENCE DIRECT®
International Journal of Heat and Mass Transfer 49 (2006) 1004–1014
International Journal of HEAT and MASS TRANSFER
www.elsevier.com/locate/ijhmt

Heat and mass transfer and condensation interference in a laminar flow diffusion chamber

S.P. Fisenko *, A.A. Brin

A.V. Luikov Heat and Mass Transfer Institute, National Academy of Sciences of Belarus, 15 P. Brovka St., Minsk 220072, Belarus

Received 15 July 2005
Available online 14 November 2005

Abstract

New mathematical model of laminar flow diffusion chamber (LFDC) performance is proposed, which includes mutial influence of homogeneous (heterogeneous) nucleation and droplets growth on heat and mass transfer processes. Qualitative investigation of heat and mass transfer processes and their influence on droplets growth is made. The limits of applicability of earlier mathematical model of LFDC are established. The numerical simulation of new mathematical model of the performance LFDC is presented. It is discovered that the nature of carrier gas substantially affects on the volume of nucleation zone in LFDC. In particular, for argon as the carrier gas the volume of nucleation zone is on the order above then for helium as the carrier gas. Effects of local structure of supersaturation field near growing droplets are discussed. Their application for interpretation of experimental data is proposed.

1. Introduction

Heat and mass transfer and vapor condensation interference is very pronounced for flows with nucleation. In this paper we will pay special attention only to flows in a laminar flow diffusion chamber, where hydrodynamic processes are well known and there are reliable measurements of all inlet parameters.

It must be remembered that for experimental studies of homogeneous nucleation in flows of vapor–gas mixtures, there are several types of devices. But until recently experimentalists used only the Wilson chamber, including its modifications, and diffusion cloud chambers. It is worth to note that the range of nucleation rate, studied with each of these devices do not overlap. The diffusion cloud chamber is used for measurements of relatively small nucleation rates (about 10^6 droplets/(m^3s)) in steady-state regime. Usually the Wilson chamber, which uses adiabatic expansion of vapor–gas mixture in low-pressure volume, is aimed for measurements of much higher nucleation rates. It is important that the Wilson chamber and its modifications work at an impulse regime and usually at lower temperature in comparision with diffusion cloud chamber.

For the steady-state regime a range of nucleation rates, which can be obtained in a laminar flow diffusion chamber (LFDC), usually is between these ones [1–7]. The sketch of LFDC is shown in Fig. 1. The idea of LFDC performance is that hot vapor–gas mixture (after saturator) enters into vertical cylindrical chamber (condenser) with a cold wall. There is a preliminary formed thin film of the condensate on the wall. Vapor diffusion and heat conductivity start to change the temperature, composition and averaged velocity of a mixture. As a rule, the composition of the mixture is selected in such manner that the Lewis number *Le* is greater than 1. The density of the saturated vapor exponentially depends on its temperature, therefore even little cooling of the mixture leads to the appearance of supersaturated medium in the central part of the channel. If supersaturation is relatively high, a homogeneous nucleation takes place and there is a subsequent growth of new phase droplets. For high nucleation rates, release of the latent heat of phase transition changes the temperature profiles and, correspondingly, heat and mass transfer in the system. Optical count of the number of droplets permits to

* Corresponding author. Tel.: +375 17 284 2222; fax: +375 17 232 2513.
E-mail address: fsp@hmti.ac.by (S.P. Fisenko).

0017-9310/$ - see front matter © 2005 Elsevier Ltd. All rights reserved.
doi:10.1016/j.ijheatmasstransfer.2005.09.007

Nomenclature

An	amplitude of numerical density (m^{-3})
At	amplitude of temperature (K)
b_1	minimal positive root of the equation
c	specific heat ($J\ kg^{-1}\ K^{-1}$)
c_d	specific heat of the droplet ($J\ kg^{-1}\ K^{-1}$)
c_m	specific heat of mixture ($J\ kg^{-1}\ K^{-1}$)
D	diffusion coefficient of the vapor (m^2/s)
d	width of the nucleation zone (m)
I_n	diffusion sink (s^{-1})
I_t	heat source ($K\ m^3\ s^{-1}$)
J	nucleation rate ($m^{-3}\ s^{-1}$)
J_c	isothermal nucleation rate ($m^{-3}\ s^{-1}$)
J_0	Bessel's function of the zeroth order
J_1	Bessel's function of the first order
k_1	coefficient (m^2)
k_r	coefficient ($s^{-1}\ m^2$)
kt_r	coefficient ($s^{-1}\ m^2$)
L	fitting parameter (m)
l_t	characteristic length of the decay of the temperature field (m)
l_v	characteristic length of the decay of the density field (m)
m	mass of vapor molecule (kg)
N_d	the number of droplets (m^{-3})
N_{eff}	maximum number of surviving droplets (m^{-3})
n	numerical density of vapor (m^{-3})
n_s	numerical density of saturated vapor (m^{-3})
R	radius of the condenser (m)
R_d	droplet radius (m)
R_{eff}	distance from droplets exceeds ten droplet radii (m)
R_m	highest possible droplet radius (m)
r	radial coordinate (m)
T	temperature of the vapor–gas mixture (K)
T_c	temperature of the condenser (K)
T_s	temperature of the saturator (K)
T_w	temperature of the wall (K)
U	latent heat of the phase transition per molecule ($kg\ m^2\ s^{-2}$)
u	velocity of gaseous mixture (m/s)
u_f	final velocity of the mixture (m/s)
u_0	averaged over cross-section velocity (m/s)
v_a	volume per molecule in liquid phase (m^3)
v_f	averaged velocity of flow after its cooling (m/s)
z	axial coordinate (m)
z_0	axial coordinate (m)
Kn	Knudsen number
Le	Lewis number
Re	Reynolds number

Greek symbols

$\Delta\Phi^*$	global minimum of the free energy of critical cluster formation, dimensionless
λ	thermal conductivity of mixture (W/m K)
λ_d	mean free path of vapor molecule (m)
ρ	density (kg/m^3)
ρ_l	density of liquid (kg/m^3)
ρ_m	density of mixture (kg/m^3)
σ	surface tension of propanol ($J\ m^{-2}$)
τ	characteristic nucleation time (s)

Subscripts

0	initial
d	droplet
f	final
c	condenser
s	saturator
w	wall
eff	effective
m	maximal
l	liquid
v	vapor
t	temperature

determine the dependence of the nucleation rate on many parameters of LFDC. For $Le < 1$, supersaturation will appear only near the surface of the cold film. For mixture of air–water vapor in LFDC, when $Le < 1$, detailed calculations of fields temperature and supersaturation are presented in [8].

It was established by experimentalists, the nature of carrier gas affects the LFDC performance; in particular, the number of carrier-gases was investigated at [2]. Among them were hydrogen, helium, argon and nitrogen, as a vapor 1-propanol (C_3H_8O) was used. For the same supersaturation, authors of [3] discovered a interesting fact that in LFDC, the nucleation rate of propanol with argon as the carrier gas is higher than the one with carrier-gas helium. In other words, it was experimentally discovered that a carrier gas affects the kinetics nucleation. This conclusion seriously contradicts the classical theory of the nucleation kinetics. One of the basic aims of this paper is to find a solution for this contradiction. We consider not only heat and mass transfer processes in gas phase but also processes related with droplets growth and motion in the nucleation zone, and their interference. These processes really depend on the nature of a carrier gas and the total pressure in LFDC [7].

For mixtures of higher alcohol with helium, the measurements of homogeneous nucleation rate in LFDC have

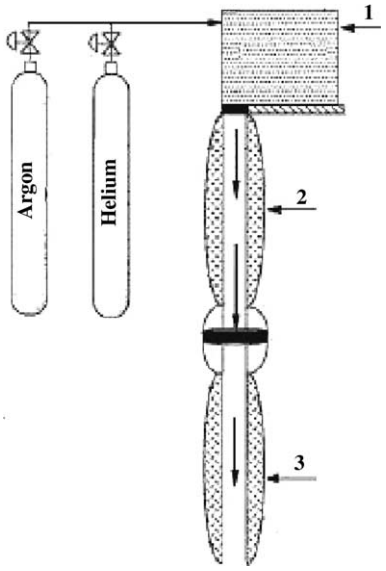

Fig. 1. Scheme of a laminar flow diffusion chamber.

been made in [4]. Discrepancy between theoretical results and the best experimental data is about three orders of magnitude of nucleation rate. Interesting fact was noted that at the measurement zone almost for 90% droplets radii were in the range 1–5 μm [5].

It is worth to emphasize that for interpretation of the results of nucleation studies, calculated fields of temperature and supersaturations play very substantial role. Below for calculations of LFDC performance we use the new mathematical model, initially presented in [9].

The applications of LFDC at different nanotechnologies will be expanded. In particular we mention covering of surface nanoparticles by different substances [8,10].

2. Mathematical model of LFDC performance

For correct performance of LFDC, the flow of the mixture vapor and carrier-gas is organized in such a manner that it is a laminar one. The Reynolds number is usually smaller than one hundred. Inlet profile of the velocity $u(r)$ of gaseous mixture is

$$u(r) = 2u_0 \cdot \left[1 - \left(\frac{r}{R}\right)^2\right],$$

where u_0 is the averaged over cross-section velocity, R is the radius of the condenser.

Convective heat diffusivity equation with heat source describes the field of temperature $T(r, z)$ of the vapor–gas mixture in the condenser

$$u(r,z)\frac{\partial T(r,z)}{\partial z} = \frac{1}{\rho_m c_m}\cdot\left[\frac{1}{r}\frac{\partial}{\partial r}\left(\lambda(r,z) r \frac{\partial T}{\partial r}\right)\right] + I_t[n(r,z) - n_s(T(r,z))], \quad (1)$$

where $\lambda(r, z)$, ρ_m and c_m are, correspondingly, coefficient of the heat conductivity, the density and the heat capacity of gaseous mixture, r and z are, correspondingly, radial and axial coordinates. $I_t[n(r, z) - n_s(T(r, z))]$ is the expression for the heat source, related with the release of the latent heat of phase transition during droplets growth, $n_s(T)$ is the numerical density of saturated vapor at temperature T.

Convective diffusion equation with source describes the field of the numerical vapor density $n(r, z)$ in the condenser

$$u(r)\frac{\partial n(r,z)}{\partial z} = \frac{1}{r}\frac{\partial}{\partial r}\left(D(T(r,z)) r \frac{\partial n}{\partial r}\right) + I_n(r,z)[n(r,z) - n_s(T(r,z))], \quad (2)$$

where $D(T(r, z))$ is the binary diffusion coefficient of the vapor, depending on the temperature, $I_n(r, z)[n(r, z) - n_s(T(r, z))]$ is the sink, describing the condensation of the supersaturated vapor on newly formed droplets. For modern LFDC, our estimations show that contribution of a thermodiffusion is a very small one. Therefore we neglect contributions of the conjugate processes in Eqs. (1) and (2).

There is the permanent condensation of a vapor on the cold wall of the condenser; therefore there is a thin film flow of condensed vapor. Respectively, the boundary conditions for vapor are

$$T(R,z) = T_w \quad \text{and} \quad n(R,z) = n_s(T_w), \quad (3)$$

where T_w is the cold wall temperature. We have two standard conditions in the center of flow

$$\frac{\partial T(0,z)}{\partial r} = \frac{\partial n(0,z)}{\partial r} = 0. \quad (4)$$

Integral term I_n at Eq. (2) is

$$I_n(r,z) = \frac{4\pi\rho_l}{m}\int_0^z N(z_0,r) R_d^2(z,z_0,r) L(R_d(z,z_0,r))\,dz_0, \quad (5)$$

where m is the mass of vapor molecule, ρ_l is the density of liquid propanol, $R_d(z, z_0)$ and $N_d(z_0, r)$ are, correspondingly, radius and number of droplets, formed near the point with coordinates (z_0, r).

At expression (5) the function $L(R_d)$ depends on the Knudsen number ($Kn = \lambda_d/R_d$, where λ_d is the mean free path of vapor molecule). This function, useful for description of the isothermal mass transfer of droplet and vapor for different regimes of droplet growth, was obtained in [11]

$$L(R_d) = \frac{Dm}{\rho_l R_d}\left(\frac{1}{1 + (D/R_d)\sqrt{2\pi m/kT}}\right),$$

where k is the Boltzmann's constant. We take into account the temperature dependence of the diffusion coefficient D.

For the number density of droplets per unit of volume $N_d(z, r)$, we have steady-state form of the continuity equation with the source, which describes nucleation contribution

$$\frac{\partial N_d(z,r)}{\partial z} = \frac{J(z,r)}{u(z,r)}, \quad (6)$$

where $J(z, r)$ is the local nucleation rate.

For description of droplets growth in a supersaturated vapor we use the equation, obtained in [11]:

$$\frac{\partial R_{\mathrm{d}}(z,z_0)}{\partial z} = L(R_{\mathrm{d}}(z,z_0))\frac{n(r,z)-n_{\mathrm{s}}(T(r,z))}{u(r,z)}. \tag{7}$$

In Eq. (1) the integral term I_{t} is

$$I_{\mathrm{t}} = U\cdot I_n/\left(\rho_{\mathrm{m}}c_{\mathrm{m}} + N4\pi R_{\mathrm{d}}^3\rho c_{\mathrm{d}}/3\right), \tag{8}$$

where U is the latent heat of the phase transition per one vapor molecule, c_{d} is the specific heat capacity of the droplet.

We assume that the inlet flow has uniform distribution of the vapor density and temperature

$$T(0,r) = T_{\mathrm{c}} \quad \text{and} \quad n(0,r) = n_{\mathrm{s}}(T_{\mathrm{s}}), \tag{9}$$

where T_{s} is the temperature of "saturator" LFDC and T_{c} is the inlet temperature of vapor–gas mixture before the LFDC condenser [2].

Before the discussion obtained numerical results, we present qualitative estimations in the next chapter [12].

3. Qualitative estimations

For obtaining of qualitative estimations of fields of the temperature and density vapor in the condenser, we approximately integrate Eqs. (1) and (2) using the Galerkin method [13]. For cylindrical condenser as the trial function, we choose the Bessel function of the zeroth order. Below we use only two first terms of the expansion of expressions for fields of temperature and of vapor density at the series of Bessel functions. Approximately the temperature field in the condenser is

$$T(r,z) = At(z)J_0(b_1 r/R) + T_{\mathrm{w}}, \tag{10}$$

where $At(z)$ is the unknown function, which will be determined later. Correspondingly, the expression for the field of the vapor density is described by similar expression with unknown function $An(z)$

$$n(r,z) = An(z)J_0(b_1 r/R) + n_{\mathrm{s}}(T_{\mathrm{w}}), \tag{11}$$

where b_1 is the least positive root of the equation

$$J_0(b_1) = 0.$$

Expressions (10) and (11) satisfy the boundary conditions (3) and (4) exactly. Substituting expressions (10) and (11) into Eqs. (2) and (3), and after simple transformations we have two ordinary differential equations for functions $An(z)$ and $At(z)$

$$2u_0k_1\partial_z An(z) = -k_r An(z),$$
$$2u_0k_1\partial_z At(z) = -kt_r At(z).$$

The solution of the first differential equation is

$$An(z) = An_0\exp\left[-\frac{z}{2u_0}\frac{k_r}{k_1}\right],$$

where $An_0 = n_{\mathrm{s}}(T_{\mathrm{s}}) - n_{\mathrm{s}}(T_{\mathrm{w}})$ and the following notations are used:

$$k_1 = \int_0^R r[1-(r/R)^2]J_0^2(b_1 r/R)\,\mathrm{d}r = 0.107R^2,$$
$$k_r = \frac{b_1^2}{R^2}\int_0^R rD(T(r))J_1^2(b_1 r/R)\,\mathrm{d}r.$$

Correspondingly, the expression for $At(z)$ is

$$At(z) = At_0\exp\left[-\frac{z}{u_0}\frac{kt_r}{2k_1}\right],$$

where $At_0 = T_{\mathrm{c}} - T_{\mathrm{w}}$ and the following notation is used:

$$kt_r = \frac{b_1^2}{R^2}\int_0^R r\frac{\lambda(T(r))J_1^2(b_1 r/R)}{\rho_{\mathrm{m}}(T(r))c_{\mathrm{m}}(T(r))}\mathrm{d}r.$$

It is helpful here to introduce the characteristic length of the decay of the temperature field l_{t}, which is directly proportional to the square of the chamber radius and the averaged velocity of flow and inversely proportional to the heat conductivity of the mixture

$$l_{\mathrm{t}} = \frac{2u_0k_1}{kt_r} = \frac{2u_0R^2\rho_{\mathrm{m}}c_{\mathrm{m}}}{\lambda(T_{\mathrm{w}})b_1^2}0.8,$$

and the characteristic length of the decay of the field of numerical vapor density l_{v}:

$$l_{\mathrm{v}} = \frac{2u_0k_1}{k_r} = \frac{2u_0R^2}{D(T_{\mathrm{w}})b_1^2}0.8.$$

It is easy to show that for mixtures with helium, $l_{\mathrm{v}} \gg l_{\mathrm{t}}$, due to high heat conductivity of helium. Calculation gives us that for mixture argon–propanol, $l_{\mathrm{v}} > l_{\mathrm{t}}$ also. To note that due to the continuity equation of the gas phase the product $u_0R^2\rho c = \text{constant}$ along the condenser. This circumstance significantly improves the efficiency of the application of the Galerkin method. In particular, for conditions of the run 1 from [2] (mixture helium–propanol) we have $l_{\mathrm{v}}/R = 4$ and $l_{\mathrm{t}}/R = 0.13$. For the same conditions for mixture argon–propanol we have $l_{\mathrm{v}}/R = 14.8$ and $l_{\mathrm{t}}/R = 10.9$.

Using the obtained above formulas, we have the approximate expression for the supersaturation field $S(r,z) = n(r,z)/n_{\mathrm{s}}(r,z)$

$$S(r,z) = \frac{(n_{\mathrm{s}}(T_{\mathrm{s}}) - n_{\mathrm{s}}(T_{\mathrm{w}}))\exp\left[-\frac{z}{l_{\mathrm{v}}}\right]J_0(b_1 r/R) + n_{\mathrm{s}}(T_{\mathrm{w}})}{n_{\mathrm{s}}\left[At_0\exp\left[-\frac{z}{l_{\mathrm{t}}}\right]J_0(b_1 r/R) + T_{\mathrm{w}}\right]}. \tag{12}$$

If $l_{\mathrm{v}} > l_{\mathrm{t}}$ and far from inlet of the condenser, where the temperature field already equalized, we have a more simple expression

$$S(r,z) = \left[\left(\frac{n_{\mathrm{s}}(T_{\mathrm{s}})}{n_{\mathrm{s}}(T_{\mathrm{w}})} - 1\right)\exp\left[-\frac{z}{l_{\mathrm{v}}}\right]J_0(b_1 r/R) + 1\right]. \tag{12'}$$

Expression (12) gives qualitatively good description of the behavior of the field of supersaturation in LFDC. Similar behavior of the supersaturation field in LFDC was numerically obtained in [2–7]. The supersaturation field in LFDC, calculated by means of expression (12), is displayed in Fig. 2.

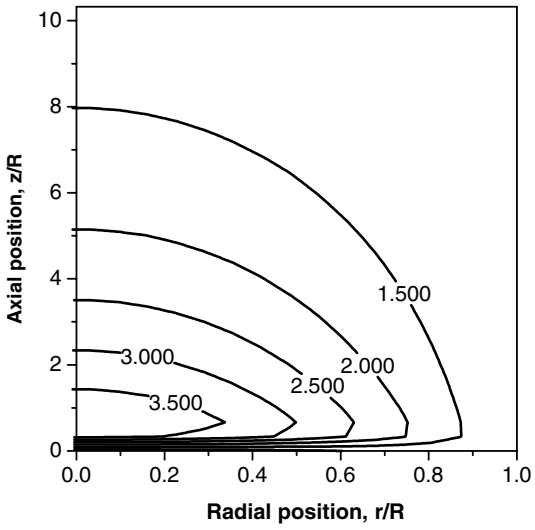

Fig. 2. Contour plot of supersaturation field.

To calculate the dimensionless free energy of critical cluster formation we use the well-known formula [2]

$$\Delta\Phi(r,z) = \frac{16\pi\sigma^3 v_a^2}{3(kT(r,z))^2(\ln S(r,z))^2},$$

where σ is the surface tension of propanol, v_a is the volume per molecule in liquid phase.

Two-dimensional field of the dimensionless free energy for propanol critical clusters is demonstrated in Fig. 3. We used the same conditions as for Fig. 2 and for Fig. 3. As seen in Fig. 3 the dimensionless global minimum of the free energy, $\Delta\Phi^*$, is on the axes of symmetry of the condenser; it is equal to $\Delta\Phi^* \approx 23$. The axial width of nucleation zone, determined by the condition that free energy at the border is equal to $\Delta\Phi^* + 2$, is about $0.6R$, and at radial direction, the width is smaller than $0.2R$. Thus we determine the actual volume of nucleation zone, in which vast majority of new droplets is formed. As we shall see later, two terms of expansion (10) and (11) determined the value of global minimum not accurately enough. Nevertheless Fig. 3 gives qualitatively correct view about the sizes of the nucleation zone.

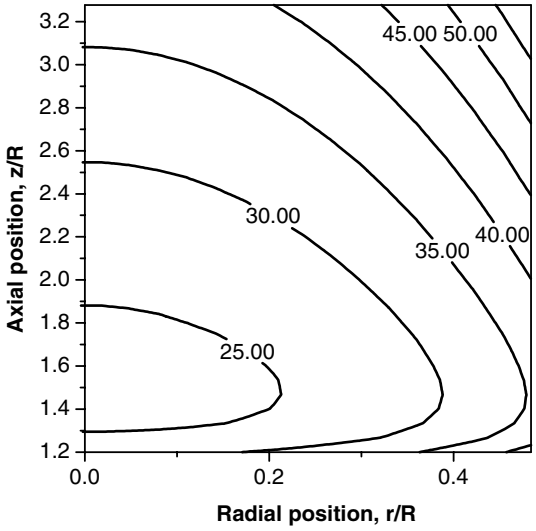

Fig. 3. Contour plot of the free energy formation of the critical clusters.

Following the estimation, obtained at [9], we can neglect the depletion of vapor due to condensation on clusters and droplets in LFCD only if for the number of droplets per volume N_d, the following inequality is valid:

$$N_d \ll R^{-2}R_d^{-1}. \tag{13}$$

In other words, we can use mathematical models of the performance of LDFC, described in [2–5]. For LDFC, described in [2], the inequality (13) means that N_d has to be much smaller than 10^9 droplets/m^3. Otherwise droplets with a radius about 1 μm substantially change the state of vapor–gas mixture (temperature and vapor density). Using Eq. (1), we can make additional estimation. In order to neglect the release of the latent heat of phase transition in LDFC, the number droplets per unit of volume has to satisfy the following inequality:

$$N_d \ll Le(U/kT_w)^{-1}R^{-2}R_d^{-1}, \tag{13'}$$

where the Lewis number Le is defined as

$$Le = \frac{\lambda}{\rho c D}.$$

Gaseous mixtures, used at LFCD, have the Lewis number greater than one, and $U/kT_w \sim 10$. For mixture of helium–propanol the Lewis number $Le \approx 31$, для mixture argon–propanol $Le \approx 1.3$. To note important results of the paper [14], where analytical calculations have been made of some parameters LFDC versus variations of inlet profile of velocity.

There is the connection between N_d and nucleation rate J. After approximate integration of Eq. (6) we have the following expression:

$$J \approx v_f N_d/d, \tag{14}$$

where d is the width of the nucleation zone in LFDC, v_f is the averaged velocity of flow after its cooling.

Let us estimate the way of growth of newly formed droplets, using Eq. (7) and the expression (12). The droplet growth stops in LFDC if supersaturation dropped to the value one. It follow from (12) that supersaturation practically dropped to one if $z/l_v = 3$. Therefore the way of droplets growth is equal to three characteristic lengths of the decay of vapor density l_v.

Approximately integrating Eq. (7), we have dependence of droplet radius versus way z on the axes of the chamber

$$R_d(z) \sim \sqrt{\left(\frac{n_s(T_s)}{n_s(T_w)} - 1\right)\frac{(D(T_w)ml_v(1-\exp(-z/l_v)}{2u_0\rho}}, \tag{15}$$

or substituting expression for l_v into (14), we have

$$R_d(z) \sim \frac{R}{b_1}\sqrt{\left(\frac{n_s(T_s)}{n_s(T_w)} - 1\right)\frac{m(1-\exp(-z/l_v)}{\rho}}.$$

Thus the highest possible droplet radius R_m in LFDC is proportional to

$$R_m(z) \sim \frac{R}{b_1}\sqrt{\left(\frac{n_s(T_s)}{n_s(T_w)} - 1\right)\frac{m}{\rho}}.$$

We see that the saturator temperature T_s substantially affect the maximum radius of droplets, formed in the LFDC. Interestingly, R_m is proportional to the radius of condenser.

4. Methods of numerical investigation

For approximate calculation of the profile of velocity mixture, which change который during cooling process, we use the following equations: Continuity equation for vapor–gas mixture

$$\rho(T_c) \cdot u_0 = \rho(T_w) \cdot u_f, \tag{16}$$

where T_w is the temperature of the cold wall of LFDC, $\rho(T_w)$ and $\rho(T_c)$ are densities of mixture, correspondingly, at temperatures T_w and T_c and atmospheric pressure, u_f is the final velocity of the mixture; also we use the equation of the state of the ideal gas. The expression for the final velocity u_f is

$$u_f = u_0 \cdot \frac{T_w}{T_c}. \tag{17}$$

For transient part of the flow in condenser, where cooling takes place, we use the simplest linear approximation for averaged velocity

$$u(z) = \begin{cases} u_0 + \dfrac{(u_f - u_0)\cdot z}{L}, & z < L, \\ u_f, & z \geqslant L, \end{cases} \tag{18}$$

where z is the current position, L is a fitting parameter. The value of L is determined by iterative procedure. The criteria for the convergence of iteration is that way of dropping temperature of the mixture on the chamber axes is equal to L. We keep assumption about the parabolic velocity of the flow [15].

For solving the system of partial differential equations and ordinary differential equations (ODE) we use semi-discrete lines method [16,17]. At the frame of this method we use the expansion into finite differences of radial derivatives. We use special methods [17], which permit correctly to take into account dependencies of transfer coefficients on temperature and vapor density [18]. Axial variable z is treated as the continuous variable. As a result of this expansion the system of partial differential equations is converted into the system of ODE. The number of new ODE is equal to the double number of knots along radial direction. Finally, we have the nonlinear system of ODE, which was solved numerically by the adaptive Runge–Kutta method of the fourth order by means of MathCAD 2000 Professional.

5. Simulation results

Some numerical results for gas phase parameters, obtained by the solution of 14 ODE are demonstrated in Figs. 4–8. Thermophysical properties of the propanol, carrier gases, values of heat conductivity coefficient and the diffusion coefficient propanol in helium and other gases are taken from [2,19]. For reckoning of the heat conductivity of binary mixture well-known method have been used [19].

For comparison, the results of application of the standard mathematical model of LFDC performance are presented in Figs. 4–9. For different radial positions, propanol vapor density profiles are displayed in Fig. 4 (helium is the carrier gas). For receiving dimensionless values the density saturated propanol vapor was used at the temperature of cold wall; the radius of the condenser of LFDC was chosen as the scale of spatial sizes. Interestingly, there is initial part of flow on the chamber axes where the vapor density does not change. Fig. 4 shows exponential dropping of the vapor density versus distance agrees well with qualitative estimations made above.

Profiles of the dimensionless temperature of propanol–helium mixture are presented in Fig. 5. The value T_w was used as the scale. We see that exponential dropping of temperature on the axes is over already for $z \approx 0.75R$. The results shown in Figs. 4 and 5, give clear understanding of the LDFC performance for the case when $Le = l_v/l_t$ is much greater than one.

Note that it follows from curves 3 in Figs. 4 and 5, that local zones of relatively supersaturation arise near the inlet of the condenser. The reason for this is the fast dropping of mixture temperature far from the center of the flow, therefore due to the exponential dependence of the saturated vapor density on temperature, we see local maximum of supersaturation. For the first time this fact was established in [2].

For conditions of two experiments from [2] the cluster growth in the condenser is shown in Fig. 6. For the mixture with helium cluster (droplet) it reaches the radius of 6 μm

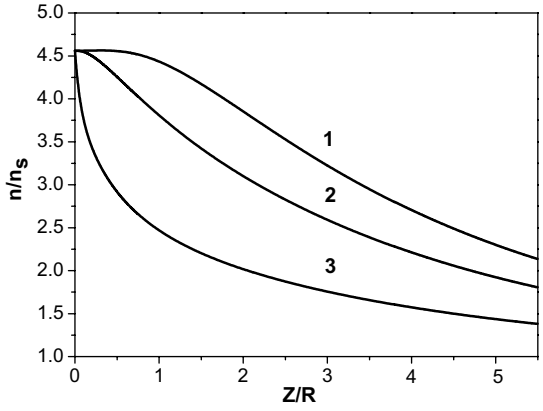

Fig. 4. Profiles of dimensionless density. Curve 1 is for chamber axis; curve 2 is for $r/R = 0.286$; curve 3 is for $r/R = 0.714$.

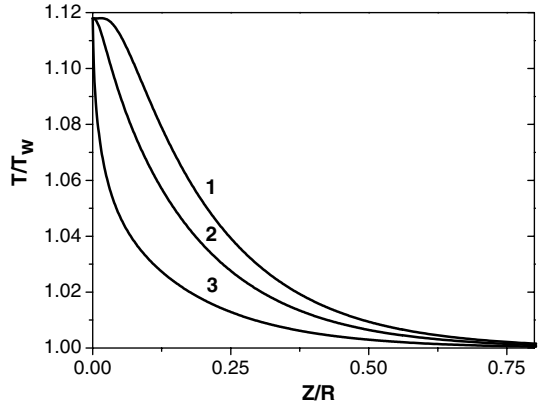

Fig. 5. Profiles of dimensionless temperature. Curve 1 is for chamber axis; curve 2 is for $r/R = 0.286$; curve 3 is for $r/R = 0.714$.

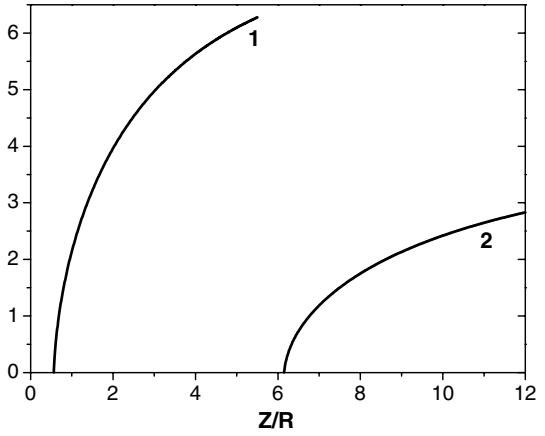

Fig. 6. Droplet growth in the condenser for different carrier gases. Curve 1 is for helium; curve 2 is for argon.

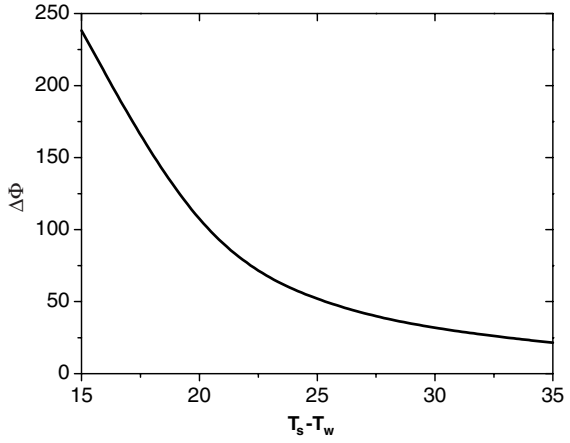

Fig. 7. Dimensionless free energy of the critical cluster formation versus temperature drop ($T_s - T_w$). Curve 1 is for chamber axis; curve 2 is for $r/R = 0.286$; curve 3 is for $r/R = 0.714$.

on the way $5R$ from the condenser inlet. For the mixture with argon droplet reaches size 3 μm on the way $6R$. To note that the droplet growth at the free molecular regime ($Kn \gg 1$) is so fast that droplet practically does not change

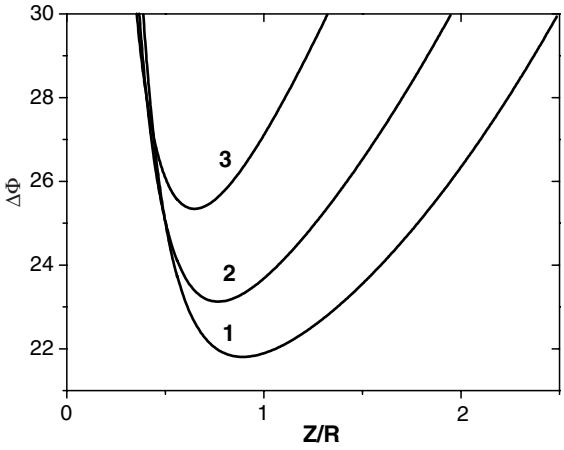

Fig. 8. Global minimum of the free energy of critical cluster formation in nucleation zone. Curve 1 is for chamber axis; curve 2 is for $r/R = 0.286$; curve 3 is for $r/R = 0.571$.

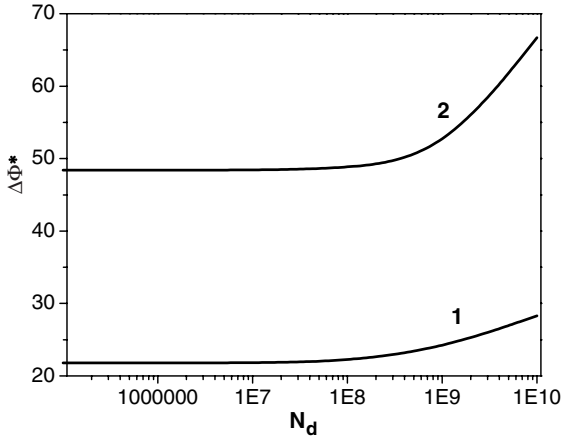

Fig. 9. Global minimum of the free energy of critical cluster formation versus total number of droplets. Curve 1 is for helium; curve 2 is for argon.

its position at the condenser. Growth of relatively large droplets runs at the diffusion regime along all chambers and it is much slower. The result of simulation agrees well with our analytic estimations.

Global minimum of the free energy of critical clusters versus temperature difference of the saturator and cold wall is shown in Fig. 7. The saturator temperature is kept constant during this simulation, and only temperature of cold wall is changed; other temperatures are constant ($T_c = 330$ K, $T_s = 322.5$ K). As it is seen from Fig. 7, if the temperature difference is smaller by 25°, the nucleation rate is very low. If we increase this temperature difference the free energy decreases. For the range temperatures shown in Fig. 7, nucleation rate has to increase on about 20 orders of magnitude. Other parameters are taken from experiment 1 from [2].

For conditions of the same experiments, dimensionless profiles of the free energy of critical cluster formation are demonstrated in Fig. 8. It is worth to pay attention to sizes of nucleation zone, where the dimensionless free energy

Table 1
Mixture of helium–propanol for Vohra and Heist [2]

N	$\Delta F_{\min}$	Z	D	S	$T_{\min}$
1(1)	21.8	0.9	1	4.4	295.4
2(5)	23.6	0.8	1	4.3	292.9
3(17)	21.2	1.1	1	4.1	301.7
4(22)	16.4	1.3	1.1	5.0	302.4
5(27)	15.0	2.1	1.5	4.9	307.4

Table 2
Mixture of argon–propanol for Vohra and Heist [2]

N	$\Delta F_{\min}$	Z	D	S	$T_{\min}$
1(28)	48.4	7.4	2.5	2.4	309.5
2(32)	43.8	8.0	2.7	2.5	311.8
3(37)	49.6	8.3	2.7	2.4	308.9
4(40)	55.2	7.6	2.4	2.3	306.9
5(44)	48.3	8.0	2.7	2.4	308.7

differs smaller than two units from the $\Delta\Phi^*$ in LDFC. Numerical results, shown in Figs. 4–9 and Tables 1 and 2, are obtained without effects of depletion, condensation on droplets and mixture heating. Obviously, if we have relatively large concentration of droplets, which occur under large supersaturation, these effects have substantial impact on the fields of vapor density and temperature.

For simulation of heat and mass transfer in LFDC with homogeneous nucleation, we insert at fixed position (z, r) some number of droplets with the same (for convenience) very small radius ($R_d \sim 2 \times 10^{-9}$ m). Thus, the number of these droplets is a free parameter at our approach. We can calculate this number, in principle, using any nucleation kinetics theory. For the first iteration we insert only one group of droplets and calculate fields of vapor density and the mixture temperature. Then, as the second iteration, we insert the next group of droplets with the same initial radius at another position before the global minimum of the free energy, calculated at previous iteration. The larger the number of iterations the more precise calculations we can do. Obviously, we simulate by such method the influence of the integral source at our mathematical model.

For the first iteration the dependence of the $\Delta\Phi^*$ in LDFC versus the total number of droplets is shown in Fig. 9. The free energy was calculated by means of capillary approximation [20]. For the first iteration at the position of inserting droplets dimensionless free energy differs from the dimensionless global minimum of the free energy, calculated by standard method, on two units. From this figure we notice that previously formed droplets changes the state of vapor–carrier gas mixture near the global minimum of the free energy. As a result the global minimum increases, and nucleation rate has to drop. As our numerical experiments show the standard mathematical model works well until the number of droplets per unit of volume is low. In particular, for conditions the run1 from [2], as it seen in Fig. 9, the number of droplets per unit of volume N_d has to be smaller than 10^8 droplets/m^3. This conclusion from

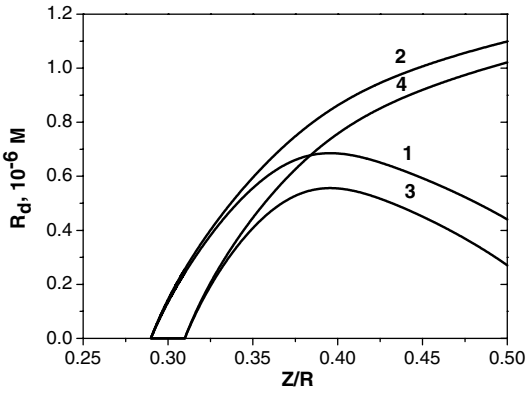

Fig. 10. Growth of two subsequent groups of clusters. First group: curve 1 is for $r/R = 0.143$; curve 2 is for $r/R = 0.286$. Second group: curve 3 is for $r/R = 0.143$; curve 4 is for $r/R = 0.286$.

simulation agrees well with the estimation (13). In order to create such number of droplets the nucleation rate has to be only about 10^9 cluster/s m^3.

For illustration of the proposed method for calculation of integral terms in our mathematical model, the growth of droplets from two different groups is shown in Fig. 10. The effect of release of latent heat of phase transition, and subsequent decreasing of supersaturation is an obvious one. The convergence of curves 2 and 4 is the manifestation of one of the effects of growth droplets at diffusion regime, discovered [21].

6. Comparison with experiments

For the mixture propanol–helium, some calculated parameters of nucleation zone are presented in Table 1. The first column gives the corresponding experiment number at the paper [2]. The second column gives the value $\Delta\Phi^*$ of propanol (as the scale we use $kT(r, z)$). The third column gives the dimensionless position of global minimum, the fourth column gives the dimensionless width of nucleation zone, the fifth column shows the maximal value of supersaturation, the sixth column gives the temperature of mixture at the position of global minimum. As it seen that very high supersaturation of propanol vapor has been reached. To remind that for all conditions observable nucleation rate was about 10^6 droplets/(m^3 s). The presented temperatures deviate from calculated results of [2] by more than 5°.

For the mixture propanol–argon, some calculated parameters of nucleation zone are presented in Table 2. We use the same meaning of columns in this table. We found that the temperature field was calculated wrongly at [2], the error could reach 5° on the axes of condenser. The radius of nucleation zone is about $2.5R$. As it is seen, the volume of nucleation zone for carrier gas argon is substantially higher, more than 5 times. The feedback between growing droplets, which move through the nucleation zone, and supersaturation value leads to substantial decreasing of the nucleation zone volume. This volume reduction is higher for experiments with helium because propanol

droplets grow much faster in this mixture. We see that the dimensionless values of the free energies of critical clusters differ significantly for experiments with argon and helium. Physical mechanisms, which lead to such results, are discussed in the next chapter.

7. Nonuniform field of supersaturation

For studies of homogeneous nucleation by means of laminar diffusion chamber, in addition to effects, discussed above, there are other kinetic effects.

The first effect is related with the local structure of the supersaturation field near to growing droplet. Significance of this effect for interpretation of high nucleation rate experiments was shown for the first time in [22]. The basic idea is the following. Supersaturation is practically equal to one on the surface of the growing droplet. It can be shown that at diffusion regime of droplet growth the supersaturation is equal to averaged one, calculated by our mathematical model, only if the distance from droplets exceeds ten droplet radii. Let us denote this distance as R_{eff}. Near growing droplet for distances smaller than R_{eff}, the supersaturation is substantially smaller than the averaged value. In other words, local structure of the supersaturation field in nucleation zone arises. Unfortunately, we cannot implement this effect at our mathematical model at reasonable manner for simulation. Therefore we limit further consideration of this effect for only semi-quantitative estimation. Formed at the beginning of nucleation zone the droplet moves through it with the velocity v_{f}. Then we have only one droplet in the cylinder with volume $v_{\text{f}}\pi R_{\text{eff}}^2$. According to the classical nucleation theory, in this cylinder has to be formed $J_{\text{c}}v_{\text{f}}\pi R_{\text{eff}}^2$ droplets, where J_{c} is isothermal nucleation rate [20]. Described above effect of local structure of supersaturation field is small for low nucleation rates. Indeed, if

$$J_{\text{c}}\pi R_{\text{ef}}^2 v_{\text{f}} \ll 1, \tag{19}$$

we can neglect this effect. For high nucleation rate this effect is a substantial one, probably not only for LDFC but also for other devices. Using data, shown in Fig. 6, we can estimate that $R_{\text{eff}} \sim 20$ μm, and $v_{\text{f}} \sim 5 \times 10^{-2}$ m/s. Then for a modest LDFC nucleation rate $J_{\text{c}} \sim 10^{12}$ cluster/(m^3 s), in the domain with characteristic radius R_{eff}, instead of 60 droplets only one droplet exists. For this example we have almost two orders of discrepancy between classical nucleation rate and observations. This effect is stronger for mixture propanol–helium, in comparison with the case when carrier gas is argon.

For very high vapor supersaturation, researchers have to take into account another effect of local field supersaturation on smaller scale, which is about the mean free path of vapor molecules. Indeed, for very high nucleation rate, we have high number density of clusters per unit volume. In this case we cannot consider the growth of each cluster independently from the neighboring clusters. To denote the mean distance between clusters as d, we have estimations

$$d \sim 1/N_{\text{d}}^{1/3}.$$

If d is about the mean free path of vapor molecules λ, neighboring clusters definitely affect on growth process. We have the following expression for N_{d}:

$$(1/N_{\text{d}})^{1/3} \sim \lambda. \tag{20}$$

For the fulfillment of the condition (20), the nucleation rate J has to be about

$$J \sim N_{\text{d}}/\tau, \tag{21}$$

where characteristic nucleation time τ is taken about 10^{-6} s [23], whereas under atmospheric pressure for propanol λ is about $\sim 10^{-6}$ m. In order to have a significant second effect from expression (21) we have the estimation of nucleation rate: $J \sim 10^{23}$ clusters/(m^3 s). Due to the stochastic nature of formation of new phase clusters, these clusters have some temporal delay and are distributed not perfectly uniform. Let us imagine that some cluster starts to grow faster than the neighboring ones. This cluster suppresses growth of the neighboring clusters for a variety of reasons. At first it is the coalescence [22,24,25], as well as release of the latent heat of phase transition. More large clusters have smaller heating rate due to larger heat capacity. Estimations, based on classical nucleation theory, show that there was such supersaturation in experiments with helium and hydrogen at [2]. We estimate the maximum number of surviving droplets N_{eff} in LDFC as following:

$$N_{\text{eff}} \approx 0.04R^2/R_{\text{eff}}^2,$$

where we consider the radius of nucleation zone $0.2R$. As characteristic radius of propanol droplet is about ~ 2 μm (helium is carrier gas), we have for experiments in [2] estimation $N_{\text{eff}} \sim 10^4$ clusters. Nucleation rate, calculated according to (14) for such number of droplets, gives the rate approximately equal to 10^6 droplets/(m^3 s). This estimation agrees well with experimental data [2].

Extrapolation of recent experimental data about propanol nucleation rates, obtained by nonsteady method [26], confirms our point that at experiments, described in [2], huge nucleation rates were reached. These rates were higher than 10^{22} clusters/(m^3 s). It also was confirmed in [26] that the nature of carrier gas did not affect the nucleation rate. It should be emphasized that diffusion interaction between growing clusters [22,24], when vast majority of small clusters disappeared, lead to the restoration of profiles of vapor density and temperature in nucleation zone of LDFC, thus effectively expanding limit of application of our mathematical model. Note that the mean free path of propanol molecules in helium is several times larger than in argon. Therefore the second effect, related with local structure of supersaturation field, is less probable if we use argon as carrier gas. Thus we proposed explanation of paradoxical experimental results, which take into account a local structure of supersaturation field. We explain the fact that nucleation rate of propanol is higher

in argon than in helium [2–4] by diffusion interaction between growing clusters and the value of nucleation zone.

8. Discussion of results

The new mathematical model of a laminar flow diffusion chamber performance (LFDC) is presented. This model permits to take into account the change parameters of the nucleation zone of a LDFC due to interference of heat and mass transfer and volume condensation process. Semi-qualitative estimations are made, based on the Galerkin's method. Our mathematical model describes effects of droplets growth at the whole range of the Knudsen numbers. It is worth to note that our mathematical model also permits to calculate the рассчитывать heterogeneous nucleation в LFDC. An example of such calculation is presented in [8].

We developed the iterative algorithm for obtaining the self-consistent solution, which describes the flows with homogeneous nucleation in LFDC. During simulation it was discovered that near the inlet of condenser LFDC there is a finite size zone near the global minimum of free energy of the propanol critical cluster $\Delta\Phi^*$, the so called nucleation zone. The volume of this nucleation zone substantially depends on thermophysical properties of carrier gas. In particular, for approximately the same conditions the volume nucleation zone with carrier gas argon is much larger than for carrier gas helium.

It was shown that investigation of homogeneous nucleation in laminar flow diffusion chamber (LFDC) could be applied only for relatively low nucleation rates. The limits of applicability are established. It was shown that the number droplets per unit of volume N_d has to satisfy the condition:

$$N_d \ll Le(U/kT_w)^{-1}R^{-2}R_d^{-1}.$$

If this inequality is not valid, growth droplets in the beginning of the nucleation zone, with relative flow of gaseous mixture, lead to increase of temperature and vapor depletion at the central part of the flow. As a result of this increasing temperature we have two effects: a decrease in the volume of nucleation zone and an increase of global minimum of free energy cluster formation in LFDC. The last effect is displayed in Fig. 9. Even relatively little increasing of the temperature manifests itself at the dropping of the total number of droplets, which can grow to the optically detectable size (about 1 μm).

Using standard mathematical model of LFDC leads to the important fact that maximum of nucleation rate should be near the axes of condenser. For relatively high supersaturation our calculations shown the central part of the condenser is the most heated part of the condenser. A shift of maximum of nucleation rate from axes means that we, at least, cannot apply standard mathematical model. For regime with high nucleation, the profiles of temperature in LFDC are shown in Fig. 11. For the number of droplets

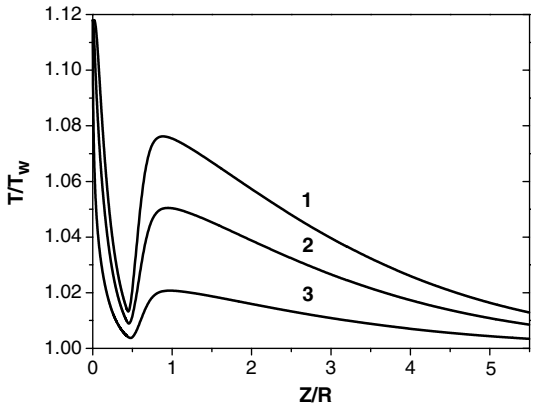

Fig. 11. Profiles of dimensionless temperature for high nucleation rates. Curve 1 is for chamber axis; curve 2 is for $r/R = 0.286$; curve 3 is for $r/R = 0.714$.

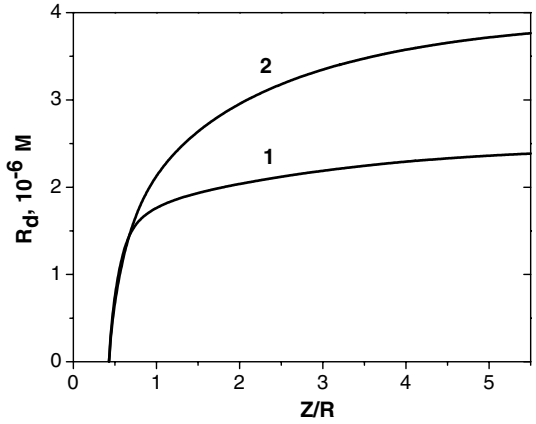

Fig. 12. Droplet growth for high nucleation rates. Curve 1 is for $r/R = 0.143$; curve 2 is for $r/R = 0.286$.

2×10^{10} per unit of volume the droplets growth is demonstrated in Fig. 12. The increasing of temperature in the central part manifests itself in more slow droplets growth.

The careful comparison of experimental results and calculated ones shown that there are additional mechanisms, which affect nucleation rate. We discussed the effects of local structure of the supersaturation field. We presented some qualitative estimations effects of local structure, which permit to explain a number of paradoxical experimental results during nucleation research with LDFC about the influence of the nature of carrier gas. Quantitative investigation of these effects is the problem of future researches.

References

[1] M.P. Anisimov, V.G. Kostrovskii, M.S. Shtein, Creation of dibutilftalat supersaturated vapor and aerosol by mixing by means of molecular diffusion flows with different temperatures, Kolloidn. Zhurnal 40 (1) (1978) 116–121 (in Russian).

[2] V. Vohra, R.H. Heist, The flow diffusion nucleation chamber: a quantitative tool for nucleation research, J. Chem. Phys. 104 (1996) 382–395.

[3] H. Lihavainen, Y. Viisanen, A laminar flow diffusion chamber for homogeneous nucleation studies, J. Phys. Chem. 105 (2001) 11619–11629.
[4] H. Lihavainen, Y. Viisanen, M. Kulmala, Homogeneous nucleation of *n*-pentanol in a laminar flow diffusion chamber, J. Chem. Phys. 114 (2001) 10031–10038.
[5] H. Lihavainen, Y. Viisanen, M. Kulmala, Homogeneous nucleation rates of higher *n*-alcohols measured in a laminar flow diffusion chamber, J. Chem. Phys. 120 (2004) 11621–11633.
[6] V.B. Mikheev, P.M. Irving, N.S. Laulainen, Laboratory measurement of water nucleation using a laminar flow tube reactor, J. Chem. Phys. 116 (2002) 10772–10786.
[7] D. Brus, A.P. Hyvärinen, V. Ždimal, H. Lihavainen, Homogeneous nucleation rate measurements of 1-butanol in helium: a comparative study of a thermal diffusion cloud chamber and a laminar flow diffusion chamber, J. Chem. Phys. 122 (2005) 214506.
[8] A.A. Brin, S.P. Fisenko, Heterogeneous condensation of water vapor on nanoparticles in a laminar flow diffusion chamber, J. Eng. Phys. Thermophys., in press.
[9] S.P. Fisenko, Simulation of laminar flow chamber for high nucleation rates, in: M. Kasahara, M. Kulmala (Eds.), Proceedings of the Sixteenth International Conference on Nucleation and Atmospheric Aerosols, Kyoto University Press, 2004, pp. 264–267.
[10] D.B. Kane, M.V. Johnston, Enhancing the detection of sulfate particles for laser ablation aerosol mass spectrometry, Anal. Chem. 73 (22) (2001) 5365–5369.
[11] D.B. Kane, S.P. Fisenko, M. Rusyniak, M.S. El-Shall, The effect of carrier gas pressure on vapor phase nucleation experiments using thermal diffusion cloud chamber, J. Chem. Phys. 111 (18) (1999) 8496–8502.
[12] V.P. Krainov, Qualitative Methods in Physical Kinetics and Hydrodynamics, American Institute of Physics, New York, 1992.
[13] C.A.J. Fletcher, Computational Galerkin Method, Springer, New York, 1984.
[14] C. Housiadas, F.E. Larrode, Y.J. Drossinos, Convective diffusion in a tube with non-uniform inlet conditions, J. Aerosol Sci. 31 (2000) 959–968.
[15] L.D. Landau, E.M. Lifshitz, Fluid Dynamics, Pergamon, London, 1987.
[16] B.S. Petukhov, Heat Exchange and Resistance in Laminar Flow of a Liquid in Tubes, Energiya, Moscow, 1967 (in Russian).
[17] V.M. Verzhbitsky, Foundations of Numerical Methods, V. Schkola, Moscow, 2002 (in Russian).
[18] J.H. Ferziger, H.G. Kaper, Mathematical Theory of Transport Processes in Gasses, North-Holland Publishing Company, Amsterdam, 1972.
[19] R.C. Reid, J.M. Prausnitz, B.E. Poling, The Properties of Gases and Liquids, McGraw-Hill, New York, 1987.
[20] Y.I. Frenkel, Kinetic Theory of Liquids, Dover, New York, 1955.
[21] Y. Vitovets, N.V. Pavlukevich, J. Smolik, S.P. Fisenko, Motion and growth of new-phase particles formed in a thermodiffusion chamber, J. Eng. Phys. Thermophys. 56 (1989) 648–652.
[22] S.P. Fisenko, R. Heist, Puzzle of high pressure nucleation experiments in diffusion cloud chambers, in: J. Schmelzer (Ed.), Nucleation Theory and Applications, Joint Institute of Nucleation Research, Dubna, 2002, pp. 146–164.
[23] S.P. Fisenko, G. Wilemski, Binary nucleation kinetics of vapors in cluster size and composition space, Phys. Rev. E 70 (2004) (056119).
[24] E.M. Lifshitz, L.P. Pitaevskii, Physical Kinetics, Pergamon, Oxford, 1981.
[25] G. Madras, B.J. McCoy, Distribution kinetics theory of Ostwald ripening, J. Chem. Phys. 115 (2001) 6699–6706.
[26] J. Wedekind, K. Iland, P.E. Wagner, R. Strey, Homogeneous nucleation of 1-alcohol vapors, in: M. Kasahara, M. Kulmala (Eds.), Proceedings of Sixteenth International Conference on Nucleation and Atmospheric Aerosols, Kyoto University Press, 2004, pp. 49–52.